RESEARCH ARTICLE

Constructal Design Applied to an Overtopping Wave Energy Converter Locate on Paraná Coast in Brazil

Sthefany Amaral da Silva [1], Jaifer Corrêa Martins [2], Elizaldo Domingues dos Santos [2], Luiz Alberto Oliveira Rocha [2], Bianca Neves Machado [3], Liércio André Isoldi [2], Mateus das Neves Gomes [1]

[1] *Paranaguá Campus, Paraná Federal Institute of Education, Science and Technology (IFPR), Paranaguá 83215-750, PR, Brazil*

[2] *School of Engineering, Federal University of Rio Grande (FURG), Rio Grande 96201-900, RS, Brazil*

[3] *Interdisciplinary Department, Federal University of Rio Grande do Sul (UFRGS), Tramandaí 95590-000, RS, Brazil*

ABSTRACT

This research aims a numerical and geometrical investigation about an Overtopping Device Wave Energy Converter (OTD-WEC). Constructal Design method was employed to perform a geometric evaluation of this OTD-WEC submitted to ocean waves with similar characteristics of the coastal region of Paraná State – Pontal do Paraná city in southern Brazil, located 41 km from the coast and 30 m water deep. It was analyzed two different significant wave heights, H_{S1} = 1.25 m and H_{S2} = 1.50 m. In each set, it were simulated 10 cases with different ramp angles, totaling 20 numerical simulations. The main goal was to evaluate the influence of the ramp angle on the water mass flow rate entering the reservoir. Therefore, through the Construtal Design, the degree of freedom (DOF) H_1/L_1 (ratio between the height and length of the ramp) was varied, considering a constant area of the ramp. For the numerical analysis, a two-dimensional computational model was employed using the commercial software Ansys Fluent, which is based on the Finite Volume Method (FVM). The multiphase Volume of Fluid (VOF) model was applied to tackle with the water-air interaction. The results showed that the best geometric configurations happened for those cases with smaller ramp angles. In addition, a reconfiguration of the ramp angles, keeping the area fixed, allowed a

*CORRESPONDING AUTHOR:

Mateus das Neves Gomes, Paranaguá Campus, Paraná Federal Institute of Education, Science and Technology (IFPR), Paranaguá 83215-750, PR, Brazil; Email: mateus.gomes@ifpr.edu.br

significant improvement in the OTD-WEC available power.

Keywords: Numerical Simulation; Geometric Analysis; Sea Wave Energy Converter; Overtopping Device; Ansys Fluent

1. Introduction

Electric energy is a very important resource nowadays, as it provides comfort and well-being, which in turn becomes indispensable for life in society; in addition, it is fundamental for the development of industries and commerce in general. Besides that, the energy issue in the environmental context is relevant[1]. Over the last several decades, the world's emerging countries have seen significant increases in their growth rate. The energy sector's contribution is considered particularly impressive in the process of fast economic growth[2].

A raised concerns over climate change, global warming, and energy security have led to increased use of renewable energy resources over the last years[3]. In light of this, among the types of renewable energy sources is ocean energy, which can be didactically divided according to its origin. The main types are: wave energy, tidal energy, temperature gradient, and salinity gradient. Therefore, the increased need for in the recent decades has resulted in a significant growth in the research and development of Wave Energy Converters (WEC) with the goal of meeting the escalating demand for clean and renewable energies, through the conversion of the ocean wave energy into electricity[4, 5].

One of the devices that convert the energy of ocean waves into electrical energy is the Overtopping Device Wave Energy Converter (OTD-WEC), which can be floating or fixed, installed on offshore, nearshore, or onshore location in the sea. The physical operating principle of the OTD-WEC consists of a ramp on which the incident waves are taken to a reservoir located above mean sea level, and then the accumulated water returns to the sea and consequently drives a turbine coupled with electrical generators, thus producing electrical energy[6, 7].

In this context, the main goal of this research is to numerically and geometrically analyze the behavior of an OTD-WEC considering characteristics of waves on the coast of Paraná State (in southern Brazil), located 41 km from the coastline at a depth of 30 m (called point 30), as analyzed in[8] and illustrated in **Figure 1**.
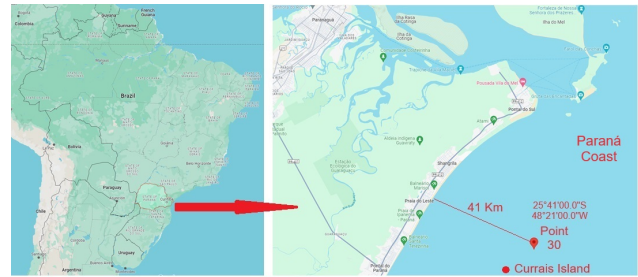
Figure 1. Location of the point 30 at Paraná Coast.

According[9], in the Brazil Southern are available the greatest mean wave power, reaching near to 40 kW/m. And the Paranaguá Campus from Federal Institute of Paraná (institution to which some of the authors of this article belong) is located at the Paraná Coast. For this reason it was choice this point to analyze. In addition, it is important to mention that in the city of Paranaguá is located the Port of Paranaguá, also called Port Dom Pedro II, which is the largest port exporting agricultural products in Brazil, with emphasis on soybeans and soybean meal. The Port of Paranaguá is the largest bulk port in Latin America. It is also the third largest container port in Brazil. It is the largest port in Brazil for grain exports. It exports and imports grains, fertilizers, containers, liquids, automobiles, wood, paper, salt, sugar, among others. Therefore, due to these reasons it is evident the relevance of oceanic and coastal activities in this geographical area, justifying an investigation regarding the harness of the ocean wave energy.

Several studies addressed to the OTD-WEC have been carried out in recent decades, approaching the problem experimentally and computationally. Recently, a research was performed in[10] about the state of the art of scientific studies dedicated to the Overtopping device used to convert sea wave energy into electrical energy, by means the Bibliometric methodology.

A way of computational approach is through the

Volume of Fluid (VOF) method[11]. This method has been widely used for numerical simulations on OTD-WEC, such as in[12–15]. In these investigations[12–15] the main purpose was to analyze, with numerical simulation, different wave conditions and different ramp parameters from OTD-WEC. It is important to highlight that this computational model was previously validated and verified considering as benchmark experiments and theoretical equations[12–15].

In addition, to perform a geometrical analysis of the OTD-WEC the Constructal Design[16–19] will be applied. As possible to observe in[10] that some papers were published about the Constructal Design method application to evaluate the OTD-WEC geometric parameters[20–26]. In general the studies from[20–26] analyzed the effect of ramp slope parameters from OTD-WEC with the main purpose to maximize the water raising in the reservoir. These investigations showed that a little change geometric parameters affects significantly increase efficiency.

For example, in[20] the ramp slope optimization leads to efficiency twenty times better than worst performance. Additionally,[22] showed that the optimal shape has a strong dependence of the relative depth. Moreover,[23] states there is no universal shape that leads to the best performance of an OTD-WEC for several conditions. This conclusion reinforced the need to analyze the geometrical and physical conditions of each case, such as the installation location of the OTD-WEC.

A study performed by[25] deepened the conclusion of[22]. The investigation of[25] showed for fixed magnitudes of distance between the bottom of the wave channel, the highest magnitudes of P_d (dimensionless available power) are achieved for the lowest possible ratio of H_1/L_1 (where H_1 is ramp height and L_1 is ramp length). For smaller construction areas of the ramp, intermediate magnitudes of distance between the bottom of the wave channel led to the highest magnitudes of P_d, i.e., the sinking of device does not led necessarily to the best performance. Moreover, optimal shapes are not universal (the same) for the two wave conditions studied.

In[26] results showed that a device with a two-ramps configuration presented an average dimensionless overtopping flow 6.48% higher than those obtained for the one ramp. The results obtained using the Con-structal Design generate theoretical recommendations about the influence of a complex configuration with four degrees of freedom over the performance of an OTD-WEC integrated into the east breakwater of the city of São José do Norte, State of Rio Grande do Sul (RS), Brazil.

It is worth mentioning the investigation of this kind of device[20–26] has been restricted to the coasts of Rio Grande do Sul and Santa Catarina states, which have another sea state conditions from Paraná state coast. For all this, the highlights in present study is to analyze the best slope ramp submitted to the ocean waves with similar characteristics of the coastal region of Paraná State. This way it will be possible to design an OTD-WEC with the best use of the region's waves. Therefore, the main innovative aspect of this paper was the application of the Constructal Design method to evaluate the geometry of an OTD-WEC over its performance in a specific region from Brazil (Paraná state coast).

2. Mathematical Modeling

The computational domain used in the numerical simulation consists of an OTD-WEC located at the end of the wave channel, **Figure 2**, installed in the coastal region of Paraná State – Pontal do Paraná city in southern Brazil, located 41 km from the coast and depth h = 30 m, as showed in **Figure 1**. This computational model is a simplification from original physical phenomenon because it is considered onshore and the point indicated in **Figure 1** is nearshore. It is possible to apply this simplification because the ocean waves characteristics are kept the same and the main purpose is to analyze the OTD-WEC slope ramp.
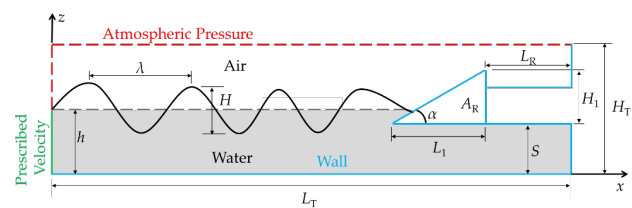
Figure 2. Illustration of the 2D computational domain.

The mean characteristics of the ocean waves at this location are detailed in **Table 1**. In the present investigation, two sets of analysis will be considered, as also shown in **Table 1**.

It is worth to mention that according to explained in [8], the wave climate at point 30 in the summer is very similar in the others seasons of the year (spring, fall and winter). So, because this reason it was chosen the summer for performed the analysis. Furthermore, the summer season is predominant on the coast of Paraná. Moreover, on the south coast of Brazil, the wave climate is affected by the South Atlantic wind pattern; being the higher energy winds over the sea surface on the south coast of the Brazilian coast are a consequence of the passage of extratropical cyclones.

Table 1. Wave characteristics of sets 1 and 2 in summer [8].

	SUMMER	
	Set 1	**Set 2**
Period (T)	8.0 s	8.0 s
Wavelength ()	95.96 m	95.96 m
Significant Wave Height (H_S)	1.25 m	1.25 m
Water Depth (h)	30.0 m	30.0 m
Incident Wave Power (P_{INC})	22,203.91 W	31,973.63 W

To calculate the wavelength in **Table 1** is applied the following equation defined by [27]:

$$\lambda = \frac{gT^2}{2\pi} tanh\left(\frac{2\pi h}{\lambda}\right) \tag{1}$$

where: g is the acceleration of gravity (m/s^2), T is the period (s), h is the water depth (m), and λ is the wavelength (m). And to obtain the Incident Wave Power (P_{INC}) is used this equation defined by [28]:

$$P_{INC} = \frac{\rho g A^2 \omega}{4k}\left(1 + \frac{2k}{sinh\left(2kh\right)}\right) \tag{2}$$

where: ρ is the density of the water (kg/m^3), A is the amplitude of the wave (m), given by $H/2$, k is the wave number given by $2\pi/\lambda$ and ω is the frequency (rad/s) given by $2\pi/T$.

Some dimensions in computational domain (see **Figure 2**) are kept fixed, similar to [25]: H_T = 37.0 m (channel height), S = 26.0 m (submergence depth), L_R = 10.0 m (reservoir length); while L_T (channel length) is variable and defined by:

$$L_T = 2\lambda + L_1 + L_R \tag{3}$$

where L_1 (ramp length) will be defined in the next section.

2.1. Constructal Design Applied to the OTD-WEC

In the present study with the application of the Construtal Design [16–19], two constraints appear: the area of the ramp (A_R), and a dimension limitation to ensure the device does not drop below the average water level, being mathematically defined, respectively, as:

$$A_R = \frac{L_1 H_1}{2} \tag{4}$$

$$(S + H_1) > (h + H_S/2) \tag{5}$$

As shown in **Table 1**, it was considered two significant wave heigh: H_{S1} = 1.25 m and H_{S2} = 1.50 m. Therefore, A_R is kept fixed and is defined by the follow relation:

$$A_R = \frac{\lambda_i H_i}{2} \tag{6}$$

where i = 1, 2 represent the respective set in **Table 1**.

Also, to apply Constructal Design is necessary to define at least a degree of freedom and a performance indicator. For this research, the main goal is to evaluate the influence of the ramp angle on the water mass flow rate that enter into reservoir. In this case the degree of freedom is defined by H_1/L_1 (where: H_1 is ramp height and L_1 is ramp length), while the performance indicator is the efficiency relation [24], given by:

$$\epsilon = \frac{P_d}{P_{INC}} \tag{7}$$

where: P_{INC} is defined in Equation (2) and P_d is given by [25]:

$$P_d = \frac{gh_a\left(t_f\right)}{t_f - t_i} \int_{t_i}^{t_f} \dot{m}_i dt \tag{8}$$

where $\dot{m}_i$ is the mass flow rate (kg/s), h_a represents the amount of water accumulated in the reservoir (m), t_f is the final time (s), and t_i is the initial time.

In summary, **Figure 3** shows a diagram with details of the application of the Constructal Design method and the numerical simulation process. The geometric evaluation is divided into two steps: 1) Constructal Design Applied to OTD-WEC and 2) Optimization.

Initially are defined the flow system (OTD-WEC), constraints, degree of freedom, and performance indica-

tor given by Equation (7). For this geometric evaluation the degree of freedom H_1/L_1 is varied.

As presented in **Figure 3**, Step 1, the maximum value found for the efficiency ϵ, Equation (8), is called the efficiency once maximized, ϵ_m, and the corresponding H_1/L_1 is called the once optimized ratio H_1/L_1, $(H_1/L_1)_o$.
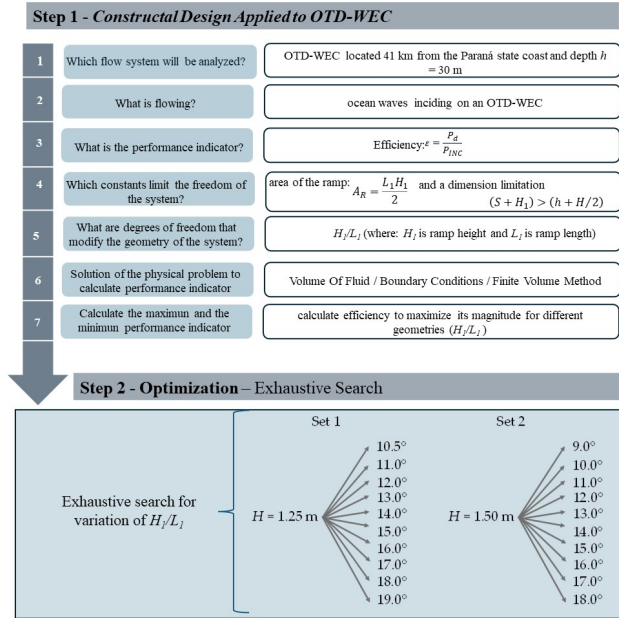
Figure 3. Diagram of the constructal design method and exhaustive search applied to the problem.

The analysis were divided in two sets according data from **Table 1** and shown in **Figure 3**, Step 2. To perform the exhaustive search of the angle due to the variation of H_1/L_1, as shown in **Figure 3**, it is necessary to employ the follow equation:

$$\theta = arctan\left(\frac{H_1}{L_1}\right) \qquad (9)$$

The angles values in **Figure 3** are different because they depend of the ocean wave characteristics, Equation (6). For example, waves with higher wave heights require ramp angles with higher magnitude to avoid the height of the device be lower than the depth water plus the wave height.

2.2. The Multiphase Volume of Fluid (VOF) Model

The flow was considered laminar, incompressible, and two-phase (water and air). Due to the interaction of these two immiscible phases, the VOF multiphase model was applied. According[11], this model is employed in mixtures with two or more fluids, emphasizing that the volume of a phase cannot be occupied by the other phases.

Thus, it is necessary to define the volume fraction concept (α). For each elementary control volume in domain the sum of all phases must be equal to one. If $\alpha = 1$ the elementary control volume is full of water, when $\alpha = 0$ the elementary control volume contains only air, and if $0 < \alpha < 1$ the elementary control volume has water and air simultaneously[11, 29].

Continuity, momentum, and volume fraction equations are solved for an isothermal, laminar, unsteady, and incompressible flow (with air and water), being defined as[11, 30]:

$$\frac{\partial \rho}{\partial t} + \nabla \cdot \left(\rho \overrightarrow{V}\right) = 0 \qquad (10)$$

where: ρ is the density (kg/m³); and $\overline{V}$ is the velocity vector of the flow (m/s).

$$\frac{\partial \left(\rho \overrightarrow{V}\right)}{\partial t} + \nabla \cdot \left(\rho \overrightarrow{V}\overrightarrow{V}\right) = -\nabla P + \nabla . \overrightarrow{\tau} + \rho \overrightarrow{g} + \overrightarrow{F} \qquad (11)$$

where: P is the pressure (N/m²); $\rho \overrightarrow{g}$ and $\overrightarrow{F}$ are the buoyancy and external body forces (N/m³), respectively; and $\overrightarrow{\tau}$ is the deformation rate tensor (N/m²), which for a Newtonian fluid is given by:

$$\overline{\tau} = \mu \left[\left(\nabla \overrightarrow{V} + \nabla \overrightarrow{V}^T\right) - \frac{2}{3}\nabla \cdot \overrightarrow{V}I\right] \qquad (12)$$

where: μ is the dynamic viscosity (kg/m·s); I is a unitary tensor; and second right-hand-side term is concerned with the deviatoric stress (N/m²).

$$\frac{\partial \alpha}{\partial t} + \nabla \cdot \left(\alpha \overrightarrow{V}\right) = 0 \qquad (13)$$

Besides that, density and viscosity for the mixture have to be calculated in each elementary control volume by the following equations:

$$\rho = \alpha \rho_{water} + (1 - \alpha)\rho_{air} \qquad (14)$$

$$\mu = \alpha \mu_{water} + (1 - \alpha)\mu_{air} \qquad (15)$$

2.3. Boundary and Initial Conditions

The wave generation is performed by means the imposition of a velocity profile at the left side surface of the wave channel (green line in **Figure 2**), simulating the behavior of a wavemaker[25]. Velocity components are based on Stokes 2nd order wave theory, in the horizontal (x) and vertical (z) wave propagation directions and given, respectively, by[27]:

$$u\left(x, z\right) = \frac{Hgk}{2\sigma} \frac{\cosh k(h+z)}{\cosh kh} \cos\left(kx - \sigma t\right) + \frac{3H^2 \sigma k}{16} \frac{\cosh 2k(h+z)}{\sinh^4 kh} \cos 2\left(kx - \sigma t\right) \tag{16}$$

$$w\left(x, z\right) = \frac{Hgk}{2\sigma} \frac{\sinh k(h+z)}{\cosh kh} \sin\left(kx - \sigma t\right) + \frac{3H^2 \sigma k}{16} \frac{\sinh 2k(h+z)}{\sinh^4 kh} \sin 2\left(kx - \sigma t\right) \tag{17}$$

where H is the significant wave height (m), k is the wave number given by $k = 2\pi/\lambda$ (m^{-1}), h is the water depth (m), T is the wave period (s), $= 2\pi/T$ is the frequency (rad/s), and t is the time (s).

The superior region of the left side surface and the superior surface of the wave channel are considered at atmospheric pressure P_{abs} = 101.3 kPa (red dashed lines in **Figure 2**). In the lower and right surfaces, as well as, in the OTD-WEC surfaces (blue lines in **Figure 2**) it is imposed a non-slip and impermeability conditions ($u = w = 0$ m/s).

Initially it was considered that the water and air inside the wave channel are at rest with a depth propagation (h) equal to 30 m.

2.4. Numerical Methods

The methods and numerical parameters adopted in the simulations are shown in **Table 2**, being based on previous works[26, 31]. To solve all the proposed cases the Finite Volume Method (FVM) was used for the numerical solution[31]. The time step size was 0.01 s, as indicated in[22].

For computational analysis it was employed a two-dimensional model widely used, in special to perform a geometrical evaluation, as in[12, 13, 22, 23, 25, 26]. In[20, 24] it was considered a three-dimensional model. From these studies, one can infer that two-dimensional model adequately represent the physical phenomenon. A major limitation for the use of three-dimensional models is the longer processing time.

2.5. Discretization

Figure 4 shows the divisions made for the spatial discretization in each part of the wave channel; and **Figure 5** illustrates the refinement details of the generated mesh. It is worth to mention that the stretched mesh method was used with greater refinement in specific regions[32, 33]. Therefore, the number of rectangular finite volumes of the meshes was close to 60,000.
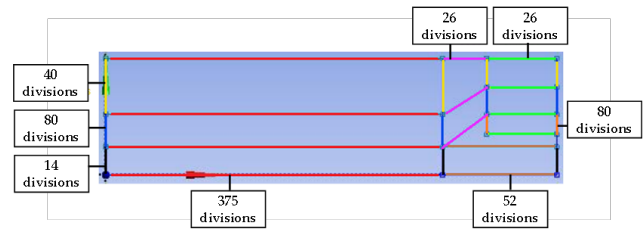
Figure 4. Illustration of the divisions of the computational domain.
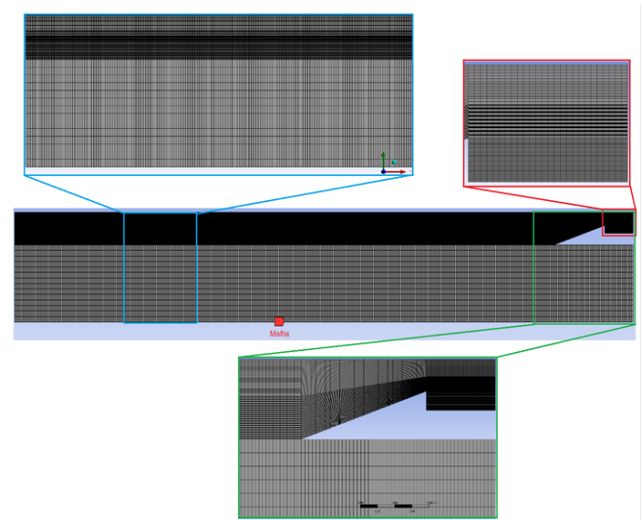
Figure 5. Illustration of the generated mesh details.

2.6. Measuring Lines

In order to monitor the elevation of the free surface and mass flow of water, some measuring lines were considered. In all, 6 lines, i.e. numerical probes, were inserted in the computational domain: a vertical line at the beginning of the numerical wave channel named S_0; 4 vertical lines inside the reservoir of the OTD-WEC, named S_1, S_2, S_3, and S_4; and a horizontal monitoring line at the superior region of the reservoir S5, as shown in **Figure 6**.

Table 2. Methods adopted in numerical simulations [26].

Parameters		Numerical Inputs
Solver		Pressure Based
Pressure-Velocity Coupling		PISO
Spatial Discretization	Gradient Evaluation	Green-Gauss Cell Based
	Pressure	PRESTO
	Momentum	First Order Upwind
	Volume Fraction	Geo-Reconstruct
Temporal Differencing Scheme		First Order Implicit
Flow Regime		Laminar
Under-Relaxation Factors	Pressure	0.3
	Momentum	0.7
Residual	Continuity	10^{-6}
	x-velocity	
	z-velocity	
Open Channel Initialization Method		Flat

Figure 6. Illustration of the positions of monitoring lines in 2D computational domain.

The S$_0$ monitoring line was positioned vertically at 10 m from the channel inlet and measures the water free surface elevation over time. It is important to highlight that the position of the numerical probes S$_1$, S$_2$, S$_3$, and S$_4$ are variable, since they depend on the geometric configuration of the device's reservoir; being used to monitor the mass flow rate. In turn, the line S$_5$ (which extends horizontally from the superior corner of the ramp to the end of the channel) is responsible for monitoring the volumetric flow of water that passes through the line, entering into the reservoir.

2.7. Wave Propagation Numerical Model Verification

For verification, initially, only the regular waves in the channel were generated, without the presence of the OTD-WEC. This step was performed twice, the first time with the significant wave height of H_{S1} = 1.25 m and the second considering H_{S2} = 1.50 m, as showed in **Table 1**.

Figure 7 presents the qualitative comparison for the numerical results obtained in monitoring line S$_0$ (see **Figure 6**) for the free surface elevation considering significant wave height of 1.25 m (**Figure 7a**) and 1.50 m (**Figure 7b**). These values were compared with the respective analytical solution (adopted as reference), being defined as [2]:

$$\eta = A\cos(kx - at) + \frac{(2A)^2 k\cosh(kh + kz)}{16\sinh^3(kh)} [2\cosh(2kh)]\cos[2(kx - at)] \quad (18)$$

To promote a quantitative comparison the indicator called numerical difference (E) was adopted, being defined as [34]:

$$E = [\sum_{n=1}^{N} |\eta_n^{Ana} - \eta_n^{Nam}|] \frac{100}{N} \quad (19)$$

where η_n^{Ana} is the water free surface elevation analytically obtained, η_n^{Nam} is the water free surface elevation numerically obtained, and N is the number of analyzed samples.

Therefore, from **Figure 7a** the numerical difference reached when H_{S1} = 1.25 m was 1.17%, while from **Figure 7b** for H_{S2} = 1.50 m a value of E = 1.50% was achieved. Furthermore, it can be seen that the numerical solution agrees with the analytical solution after approximately the first 2 s. This behavior happens because

the numerical solution needs this time to stabilize wave generation, since its initial condition considers the water in rest. This time was discounted to the numerical difference calculus.

(a)

(b)
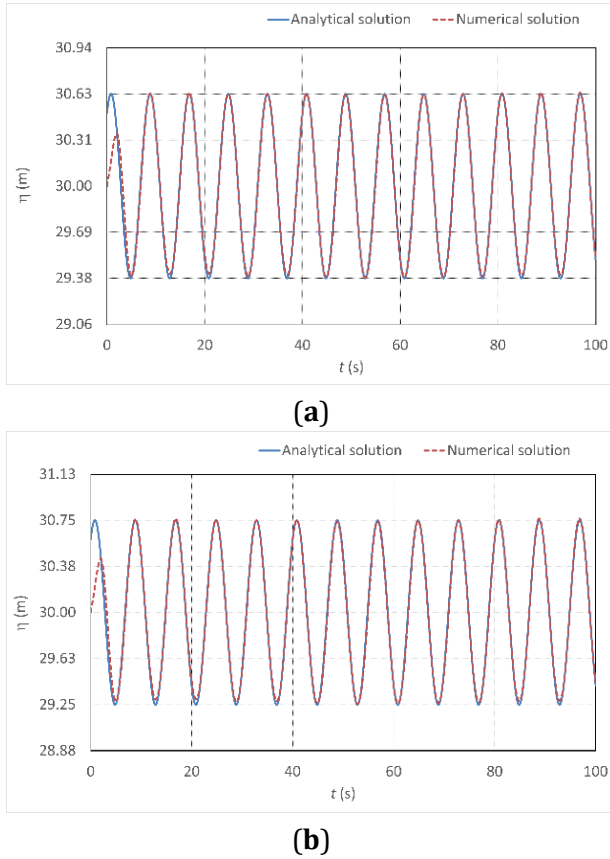
Figure 7. Free surface elevation comparison between the numerical solution and analytical solution considering significant wave height of: (**a**) 1.25 m and (**b**) 1.50 m.

2.8. OTD-WEC Numerical Model Verification

The VOF method has been widely used for numerical simulations OTD-WEC[11–14]. One can highlight that a detailed validation study about that was recently developed in[35]. Besides that, in[12–15] it were also performed validations of this numerical model to simulate an OTD-WEC. So, in the present paper the focus is just to calibrate the numerical model, aiming its application in the specific conditions of the proposed case studies.

For the calibration of the computational model, a verification of the OTD-WEC operational principle was performed by means a comparison against the case found in[25]. To do so, it was adopted the optimized ge-

ometry of[25], defined by $(H_1/L_1)_o = 0.14$ and subjected to the follow characteristics: $\lambda = 65.4$ m, $T = 7.5$ s, $H = 1.0$ m, $H_T/L_T = 0.061$, $S = 6.0$ m, and $\phi = 0.012$.

Figure 8 presented a comparison between the present study and the results from[25] for prediction of instantaneous behavior of OTD-WEC flow in the ramp for water accumulation height inside the reservoir.
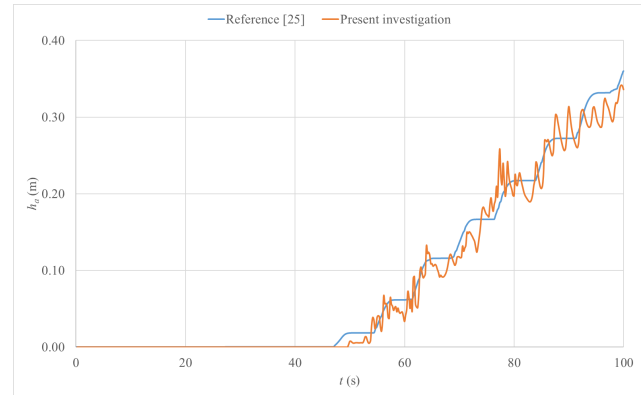
Figure 8. Transient behavior of the OTD-WEC flow in the ramp water accumulation height (*ha*) inside the reservoir.

The oscillatory behavior presented in **Figure 8** is due to the water movement inside the reservoir when the water falls into reservoir after the overtopping, as presented in[35]. Therefore, the water accumulation height (h_a) inside the reservoir is dependent from overtopping, justifying the great interest in optimize the ramp slope of the OTD-WEC.

To calibrate the numerical model in present study, it was performed a comparison considering the water accumulation height (h_a) inside the reservoir and mass flow rate, in the entering of reservoir (monitoring line S_5 in **Figure 6**). The obtained results were compared with those presented in[25].

To evaluate the difference obtained in these comparisons it was used the Root Mean Square (RMS)[36]:

$$X = \sqrt{\frac{1}{T}\int_0^T x^2 dt} \qquad (20)$$

where X is a generic variable, t is the time, and T is the considered interval time (in this case is equal to 100 s).

Table 3 presents the differences between solutions of the present study and those of[25].

Table 3. Comparison between RMS reference solution [25] and present study for mass flow rate and water accumulation height inside the reservoir.

	$(\dot{m})_{RMS}$ **(kg/s)**	$(h_a)_{RMS}$ **(m)**
Reference [24]	8.76	0.14
Present study	8.48	0.15
Difference	−0.28	0.01

One can note in **Table 3** that the differences obtained were small: $(\dot{m})_{RMS}$ = −0.28 kg/s and $(h_a)_{RMS}$ = 0.01 m. Therefore, the mathematical model implemented in the computational code is suitable for representing the physics of the problem. From this, it was possible to consider the computational model as calibrated.

3. Results and Discussion

As already mentioned, the main purpose in present investigation is to analyze the ramp slope when submitted to the ocean waves with similar characteristics of the coastal region of Paraná State that conducted the best efficiency.

To do so, were applied the wave characteristics of Pontal do Paraná, corresponding to coordinates 25° 41' S and 48° 21' W [8] named as point 30 (see **Figure 1**), considering the summer season in two sets with different wave height and incident power (**Table 1**).

In addition, the Constructal Design method was used to define possible geometric configurations by varying the degree of freedom H_1/L_1. In **Tables 4** and **5** are presented the geometric dimensions simulated (see **Figure 3**), respectively, for H_{S1} = 1.25 m (set 1) and H_{S2} = 1.50 m (set 2). These measures were obtained from Equation (4).

For both sets the constraint A_R was calculated by Equation (6), and obtained value was: A_R = 59.98 to set 1 (**Table 4**) and A_R = 71.97 to set 2 (**Table 5**). Therefore, the two sets are different and are submitted to different geometries constraints and waves conditions.

To evaluate the results it was necessary to define the ramp distance d_R, as shown in **Tables 4** and **5**. The ramp distance is the measure between the beginning of the ramp and the beginning of the reservoir, as follow:

$$d_R = \sqrt{(L_1)^2 + (H_1)^2} \qquad (21)$$

When the OTD-WEC is reached by the waves, the water is accelerate until the reservoir. So, the ramp distance d_R combined with the constraint from Equation (5) and the submergence depth S are important aspects to ensure that wave breaks slowly, overtop the ramp, and reaches the reservoir.

The results obtained in the analysis of set 1 (see **Table 4**) are shown in **Table 6**, which presents all the results of the ten cases analyzed, starting with an opening angle of 10.5° up to 19° (in which there is no overtopping).

In general, from **Table 6**, the best performance of the OTD-WEC concerning the sum of mass flow rate and amount of water accumulated in the reservoir occurs for small ratios of H_1/L_1, consequently small angles; being this finding similar with the results from [25].

However, differently from [25], in the present investigation the optimized geometric configuration for the set 1 is defined by $(H_1/L_1)_{o,set1}$ = 0.21 and occurs locally with an intermediate value for the ratio H_1/L_1. This fact is because when the angles are small, the constraint given by Equation (5) is almost to level $h + H_{S1}/2$, as shown in **Table 6**. Increasing the restriction from Equation (5) is not necessary to guarantee the best performance, as the high water level in the ramp can break the wave more quickly and not lead it to the reservoir. It is necessary a best combination between the constraint from Equation (5) and the submergence depth S.

A similar behavior can be observed to the set 2, as presented in **Table 7**. In this case, the optimal geometric configuration is defined by $(H_1/L_1)_{o,set2}$ = 0.18. Although the efficiency behavior is qualitatively similar for both sets, as depicted in **Figure 9a** and **Figure 9b**, respectively, the geometry $(H_1/L_1)_{o,set1}$ = 0.21 cannot be compared to the geometry $(H_1/L_1)_{o,set2}$ = 0.18 because they are submitted to different geometrical constraints and incident waves conditions.

All this, summarized in **Figure 9**, reinforces the need to analyze the geometry of the OTD-WEC based on the wave characteristics of the region. In this type of system, OTD-WEC, it is important to consider the ideal combination for the ramp distance d_R together with the constraint from Equation (5) and submergence depth S.

Table 4. Geometrical configurations simulated for the set 1.

H_1/L_1	$\theta°$ (Equation (9))	L_1 (m)	H_1 (m)	dR (m)	$S + H_1$ (m) (Equation (5))	$h + H_{s1}/2$ (m) (Equation (5))
0.18	10.50	25.44	4.72	25.87	30.72	30.63
0.19	11.00	24.84	4.83	25.31	30.83	30.63
0.21	12.00	23.76	5.05	24.29	31.05	30.63
0.23	13.00	22.79	5.26	23.39	31.26	30.63
0.25	14.00	21.93	5.47	22.61	31.47	30.63
0.27	15.00	21.16	5.67	21.90	31.67	30.63
0.29	16.00	20.45	5.86	21.28	31.86	30.63
0.31	17.00	19.81	6.06	20.71	32.06	30.63
0.32	18.00	19.21	6.24	20.20	32.24	30.63
0.34	19.00	18.66	6.43	19.74	32.43	30.63

Table 5. Geometrical configurations simulated for the set 2.

| H_1/L_1	$\theta°$ (Equation (9))	L_1 (m)	H_1 (m)	dR (m)	$S + H_1$ (m) (Equation (5))	$h + H_{s1}/2$ (m) (Equation (5))
0.16	9.0	30.15	4.77	30.52	30.77	30.75
0.18	10.0	28.57	5.04	29.01	31.04	30.75
0.19	11.0	27.21	5.29	27.72	31.29	30.75
0.21	12.0	26.02	5.53	26.60	31.53	30.75
0.23	13.0	24.97	5.76	25.63	31.76	30.75
0.25	14.0	24.03	5.99	24.76	31.99	30.75
0.27	15.0	23.18	6.21	23.99	32.21	30.75
0.29	16.0	22.40	6.42	23.31	32.42	30.75
0.31	17.0	21.70	6.63	22.69	32.63	30.75
0.32	18.0	21.05	6.84	22.13	32.84	30.75

Table 6. Results to set 1.

H_1/L_1	$\theta°$ (Equation (9))	$\int_{t_i}^{t_f} \dot{m}_i dt$ (kg)	h_a (m)	P_d (W) (Equation (8))
0.18	10.50	13,311.03	0.940	815.13
0.19	11.00	15,502.29	1.014	1,028.51
0.21	12.00	14,632.16	1.140	1,090.91
0.23	13.00	10,929.89	1.032	737.36
0.25	14.00	8,016.78	0.654	342.75
0.27	15.00	4,989.59	0.446	145.63
0.29	16.00	3,128.35	0.223	45.59
0.31	17.00	659.52	0.067	2.88
0.32	18.00	237.58	0.007	0.11
0.34	19.00	0.03	0.003	0.00

Table 7. Results to set 2.

H_1/L_1	$\theta°$ (Equation (9))	$\int_{t_i}^{t_f} \dot{m}_i dt$ (kg)	h_a (m)	P_d (W) (Equation (8))
0.16	9.0	14,081.71	0.930	815.50
0.18	10.0	15,484.56	1.129	1,143.08
0.19	11.0	11,573.23	0.973	736.47
0.21	12.0	7,723.41	0.738	372.89
0.23	13.0	6,008.97	0.589	231.62
0.25	14.0	4,902.34	0.459	147.29
0.27	15.0	2,571.24	0.209	35.20
0.29	16.0	1,071.96	0.078	5.46
0.31	17.0	401.27	0.011	0.30
0.32	18.0	2.68	0.001	0.00

For analysis in **Table 6**, **Table 7**, and **Figure 9** it was considered the time equal to 150 s.

(a)   **(b)**
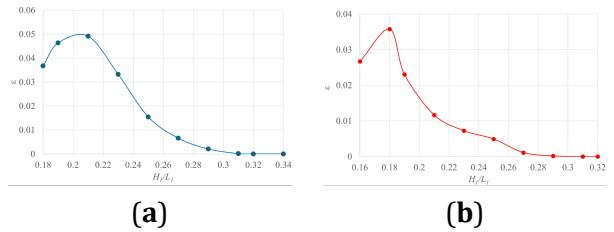
Figure 9. Efficiency variation as a function of the H_1/L_1 variation: (**a**) set 1 and (**b**) set 2.

One can infer in **Figure 9a,b** the relevance in promoting a geometric evaluation for the OTD-WEC, since for both values of incident significant wave heights its optimized geometric configuration was achieved for an intermediate value of the H_1/L_1 ratio.

In **Figure 10** is presented a comparison between different ratios H_1/L_1, (for both sets), the transient behavior water accumulation height (h_a) inside the reservoir of the OTD-WEC.

The overtopping starts nearly to 48 s, after the sixth incident wave, and the water accumulation height (h_a) inside the reservoir increase slowly.

For greatest ratios H_1/L_1 (bigger than 0.26) the water accumulation height (h_a) inside the reservoir gets

close zero, as shown in **Figure 9** and **Tables 6** and **7**. Because of that, in **Figure 10** is presented the behavior for: a) Set 1: $0.18 < H_1/L_1 < 0.27$ and b) Set 2: $0.16 < H_1/L_1 < 0.25$.

Therefore, with **Figure 10a,b**, is possible to clarify the geometry effects in OTD-WEC efficiency. Small changes in geometric dimensions can lead to large improvements in water accumulation within the OTD-WEC reservoir. The oscillatory behavior in all cases shown **Figure 10** is due the water falling movement inside the reservoir.

Comparing the results (from **Figure 10a** and **Table 6**) between $H_1/L_1 = 0.21$ and $H_1/L_1 = 0.27$ for water accumulation inside reservoir, it is possible to note an improvement about 125 % with the geometry change. A similar fact is also possible to note in **Figure 10b** and **Table 7** for set 2.
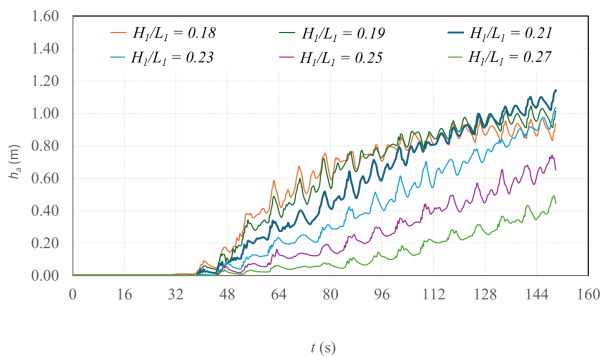
(a)
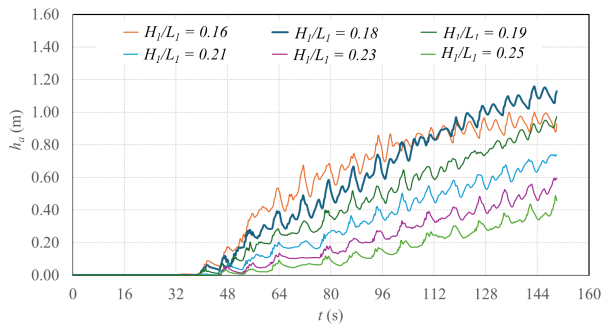
(b)

Figure 10. Transient behavior water accumulation height (ha) inside the reservoir of the OTD-WEC for different ratios H_1/L_1: (**a**) set 1 and (**b**) set 2.

4. Conclusions

In the present investigation, a numerical and geometric analysis was carried out addressed to the behavior of an OTD-WEC considering characteristics of waves from the coast of Paraná State (in southern Brazil), located 41 km from the coastline at a depth of 30 m. It were considered two set of simulations according to characteristics from the incident regular waves.

To do so, the Constructal Design method was applied to perform the geometric analysis. For the set 1 (with H_{S1} = 1.25 m) the best performance occurs locally for the optimal ratio $(H_1/L_1)_{o,set1}$ = 0.21, being different from previous result of[23]. In its turn, for the set 2 (with H_{S2} = 1.50 m) the optimized geometric configuration was achieved when $(H_1/L_1)_{o,set2}$ = 0.18. This geometric rearrangement provides a difference of up to 1000 W in available power as seen in **Tables 6** and **7**.

Finally, the results reinforced the need to analyze the geometry of the OTD-WEC based on the wave characteristics of the region, highlighting that the optimized geometries in this study were found for an intermediate value of the degree of freedom H_1/L_1. Furthermore, in this type of flow system, OTD-WEC, it is important to consider the ideal association for the ramp distance d_R combined with constraint from Equation (5) and submergence depth *S.*

From this, it was possible to perform an initial geometric evaluation concerning the OTD-WEC without the need of experimental approach, allowing with less financial costs to obtain a theoretical recommendation about the optimized configurations of its ramp slope.

In future works some additional studies can be developed, such as: (i) to submit the OTD-WEC to different depths (tidal effect); (ii) three-dimensional numerical simulation of the OTD-WEC; (iii) to consider the wave climate in other points from Brazilian South Coast; (iv) to analyze the OTD-WEC submitted to wave climate from Paraná State Coast in other seasons, (v) to consider a multi-objective optimization approach, with the purpose of maximizes the performance and also minimizes construction and maintenance costs of the OTD-WEC, and (vi) to investigate other types of WEC (such as Oscillating Water Column and Submerged Horizontal Plate) when submitted to the sea state characteristics from the coast of Paraná State.

Author Contributions

Funding

Institutional Review Board Statement

Not applicable.

Informed Consent Statement

Not applicable.

Data Availability Statement

The data presented in this study are available on request from the corresponding author. The data are not publicly available due to privacy reasons.

Acknowledgments

Conflict of Interest

The authors declare no conflict of interest. The funders had no role in the design of the study; in the collection, analyses, or interpretation of data; in the writing of the manuscript, or in the decision to publish the results.

References

[1] Hinrichs, R.A., Kleinbach, M., 2014. Energia e Meio Ambiente, 3rd ed.; Cengage Learning Editores: São Paulo. pp. 1–784.

[2] Lei, X., Alharthi, M., Ahmad, I., et al., 2022. Importance of international relations for the promotion of renewable energy, preservation of natural resources and environment: Empirics from SEA nations. Renewable Energy. 196, 1250–1257. DOI: https://doi.org/10.1016/j.renene.2022.07.083

[3] Chaoyi, C., Mehmet P., Thanasis, S., 2021. Determinants of renewable energy consumption: Importance of democratic institutions. Renewable Energy. 179, 75–83. DOI: https://doi.org/10.1016/j.renene.2021.07.030

[4] Gael, A., João, A., Fortes, C., et al., 2022. Energy assessment of potential locations for OWC instalation at the Portuguese coast. Renewable Energy. 200, 37–47. DOI: https://doi.org/10.1016/j.renene.2022.09.082

[5] Tolmasquim, M.T., 2016. Energia Renovável: Hidráulica, Biomassa, Eólica, Oceânica. Empresa de Pesquisa Energética: Rio de Janeiro. pp. 1–452.

[6] Kofoed, J., Frigaard, P., Friis-Madsen, E., et al., 2006. Prototype testing of the wave energy converter wave dragon. Renewable Energy. 31, 181–189. DOI: https://doi.org/10.1016/j.renene.2005.09.005

[7] Margheritini, L., Vicinanza, D., Frigaard, P., 2009. SSG wave energy converter: Design, reliability and hydraulic performance

of an innovative overtopping device. Renewable Energy. 34, 1371–1380. DOI: https://doi.org/10.1016/j.renene.2008.09.009

[8] Nemes, D., Marone, E., 2013. Characterization of surface waves on the inner shelf of the Paraná State. Boletim Paranaense de geociências. Paraná: Geociência. 68–69, 12–25.

[9] Rusu, L., Rusu, E., 2021. Evaluation of the Worldwide Wave Energy Distribution Based on ERA5 Data and Altimeter Measurements. Energies. 14. DOI: https://doi.org/10.3390/en14020394

[10] Paiva, M., Silveira, L., Isoldi, L., et al., 2021. Bibliometric Study Applied to the Overtopping Wave Energy Converter Device. Sustainable Marine Structures. 2(1), 35–45. DOI: https://doi.org/10.36956/sms.v2i1.306

[11] Hirt, C.W., Nichols, B.D., 1981. Volume of fluid (VOF) method for the dynamics of free boundaries. J. Comput. Phys. 39, 201–225. DOI: https://doi.org/10.1016/0021-9991(81)90145-5

[12] Liu, Z., Hyun, B.S., Jin, J., 2008. Numerical Prediction for Overtopping Performance of OWEC. IEEE. 2008.

[13] Iahnke, S.L.P., Gomes, M.N., Isoldi, L.A., et al., 2009. Energia das Ondas do Mar: Modelagem Computacional de um Dispositivo de Galgamento. Vetor. 19.

[14] Peng, Z., Zou, Q., 2011. Spatial distribution of wave overtopping water behind coastal structures. Coastal Engineering. 58(6), 489–498. DOI: https://doi.org/10.1016/j.coastaleng.2011.01.010

[15] Musa, M., Roslan, M., Ahmad, M., et al., 2020. The Influence of Ramp Shape Parameters on Performance of Overtopping Breakwater for Energy Conversion. Journal of Marine Science Energy. 8, 875. DOI: https://doi.org/10.3390/jmse8110875

[16] Bejan, A., 2000. Shape and Structure: From Engineering to Nature. Cambridge University Press: Cambridge, UK. pp. 1–362.

[17] Bejan, A., Lorente, S., 2008. Design with Constructal Design. 1. ed. Hoboken: John Wiley & Sons. pp. 1–560.

[18] Bejan, A., Zane, J., 2012. Design in Nature, Doubleday, EUA. pp. 1–304.

[19] Bejan, A., Lorente, S., 2013. Constructal Law of Design and Evolution: Physics, Biology, Technology, and Society. Journal of Applied Physics. 113. DOI: https://doi.org/10.1063/1.4798429

[20] Machado, B., 2012. Modelagem Computacional e Otimização Geométrica de um dispositivo de Galgamento para a conversão da energia das ondas do mar em energia elétrica [Master Thesis]. Federal University of Rio Grande, Brazil. pp. 1–92.

[21] Santos, E., Machado, B., Lopes, N., et al., 2013. Constructal Design of Wave Energy Converters. In: Rocha, L.A.O., Lorente, S., Bejan, A., Constructal Law and the Unifying Principle of Design, 1st Ed. Springer. pp. 275–294.

[22] Dos Santos, E., Machado, B., Zanella, M., et al., 2014. Numerical Study of the Effect of the Relative Depth on the Overtopping Wave Energy Converters According to Constructal Design. Defect and Diffusion Forum. 348, 232–244. DOI: https://doi.org/10.4028/www.scientific.net/DDF.348.232

[23] Gomes, M.N., Lara, M.F.E., Iahnke, S.L.P., et al., 2015. Numerical Approach of the Main Physical Operational Principle of Several Wave Energy Converters: Oscillating Water Column, Overtopping and Submerged Plate. Defect and Diffusion Forum. 362, 115–171. DOI: https://doi.org/10.4028/www.scientific.net/DDF.362.115

[24] Machado, B., 2016. Estudo numérico tridimensional de um dispositivo de galgamento para conversão de energia das ondas do mar em energia elétrica aplicando o método Constructal Design [PhD Thesis]. Federal University of Rio Grande do Sul, Brazil. pp. 1–143.

[25] Martins, J.C., Goulart, M.M., Gomes, M.N., et al., 2018. Geometric Evaluation of the Main Operational Principle of an Overtopping Wave Energy Converter by Means of Constructal Design. Renewable Energy. 727–741. DOI: https://doi.org/10.1016/j.renene.2017.11.061

[26] Martins, J.C., Fragassa, C., Goulart, M.M., et al., 2022. Constructal Design of an Overtopping Wave Energy Converter Incorporated in a Breakwater. Journal of Marine Science and Engineering. 10(4), 1–27. DOI: https://doi.org/10.3390/jmse10040471

[27] Chakrabarti, S.K., 2005. Handbook of Offshore Engineering. Elsevier: Amsterdan. pp. 1–661.

[28] Zhang, Y., Zou, Q., Greaves, D., 2012. Air-water two-phase flow modelling of hydrodynamic performance of an oscillating water column device. Renewable Energy. 159–170. DOI: https://doi.org/10.1016/j.renene.2011.10.011

[29] Lv, X., Zou, Q., Reeve, D., 2011. Numerical simulation of overflow at vertical weirs using a hybrid level set/VOF method. Advances in Water Resources. 34(10), 1320–1334. DOI: https://doi.org/10.1016/j.advwatres.2011.06.009

[30] Schlichting, H., 1979. Boundary-layer theory, 7th ed. McGraw-Hill: New York, USA.

[31] Versteeg, H.K., Malalasekera, W., 2007. An Introduction to Computational Fluid Dynamics: The Finite Volume Method, 2nd ed. Pearson Education: London, UK.

[32] Goulart, M.M., 2014. Estudo Numérico da Geometria de um Dispositivo de Galgamento Onshore em Escala Real Empregando Constructal Design [Master's Thesis]. Universidade Federal do Rio Grande, Rio Grande, RS.

[33] Mavriplis, D.J., 1997. Unstructured Grid Techniques, Annual Reviews Fluid Mechanics. 29, 473–514.

[34] Ferziger, J.H., Peric, M., 2002. Computacional Methods for Fluid Dynamics. 3rd. ed. Springer: Berlim.

[35] Goulart, M.M., 2022. Validação de um modelo numérico de um dispositivo de galgamento e investigação numérica e experimental da geometria aplicando o método design construtal [PhD Thesis]. Federal University of Rio Grande, Brazil. pp. 1–144.

[36] Marjani, A.E., Ruiz, F.C., Rodriguez, M.A., et al., 2008. Numerical Modeling in Wave Energy Conversion Systems. Energy. 33, 1246–1256.